Tryptophan Phosphorescence Study of Enzyme Flexibility and Unfolding in Laboratory-Evolved Thermostable Esterases†

Anne Gershenson,‡ Joseph A. Schauerte,§ Lori Giver,‡,|| and Frances H. Arnold*,‡

Division of Chemistry & Chemical Engineering, California Institute of Technology, Pasadena, California 91125, and Institute of Gerontology, University of Michigan, Ann Arbor, Michigan 48109

Received October 25, 1999; Revised Manuscript Received February 11, 2000

ABSTRACT: Directed evolution of *p*-nitrobenzyl esterase (*p*NB E) has yielded eight generations of increasingly thermostable variants. The most stable esterase, 8G8, has 13 amino acid substitutions, a melting temperature 17 °C higher than the wild-type enzyme, and increased hydrolytic activity toward *p*-nitrophenyl acetate (*p*NPA), the substrate used for evolution, at all temperatures. Room-temperature activities of the evolved thermostable variants range from 3.5 times greater to 4.0 times less than wild type. The relationships between enzyme stability, catalytic activity, and flexibility for the esterases were investigated using tryptophan phosphorescence. We observed no correlation between catalytic activity and enzyme flexibility in the vicinity of the tryptophan (Trp) residues. Increases in stability, however, are often accompanied by decreases in flexibility, as measured by Trp phosphorescence. Phosphorescence data also suggest that the N- and C-terminal regions of *p*NB E unfold independently. The N-terminal region appears more thermolabile, yet most of the thermostabilizing mutations are located in the C-terminal region. Mutational studies show that the effects of the N-terminal mutations depend on one or more mutations in the C-terminal region. Thus, the *p*NB E mutants are stabilized by long-range, cooperative interactions between distant parts of the enzyme.

Studies of naturally occurring, homologous mesophilic and thermophilic enzymes have suggested that increased thermal stability is associated with decreased enzyme flexibility (*1*). The relationship between thermostability and flexibility is, however, complex. Less flexible states are entropically costly (*2*), but this loss may be compensated for by increases in enthalpic stabilization (*3*). For example, decreased mobility can increase stability by lowering the probability of solvent penetration of the hydrophobic core which leads to unfolding (*4*). Attempts to uncover a relationship between enzyme flexibility and stability are further confounded by the possibility that other properties, such as catalytic activity, may be related to flexibility.

Most thermophilic enzymes have decreased low-temperature activity relative to their mesophilic cousins (*5*). However, when compared at their respective physiological temperatures, mesophilic and thermophilic homologues often display comparable catalytic activities and comparable conformational fluctuations (*6*−*8*). While comparable motions in the active site are likely to be associated with similar catalytic activities (*8*), conformational fluctuations outside the active site may be associated with stability and/or activity. Differentiation of the relationships between enzyme flexibility, catalytic activity, and thermostability might be achieved by studying enzymes, such as those evolved in the laboratory, which show no tradeoff between low-temperature activity and thermostability (*9*−*13*).

Bacillus subtilis p-nitrobenzyl esterase (*p*NB E),[1] a monomer of 489 amino acids, was evolved in the laboratory to increase thermostability while retaining activity at room temperature (*11*). With additional rounds of mutagenesis, recombination, and screening, we now have eight generations of related mutants characterized by increasing thermostabilities and varying catalytic activities. The X-ray crystal structures of wild-type *p*NB E and the most thermostable eighth-generation mutant, 8G8, have been determined (*14*), making this lineage particularly attractive for further biophysical characterization.

Tryptophan (Trp) phosphorescence lifetimes were used to measure the internal flexibility of wild-type *p*NB E and its thermostable variants. In the absence of oxygen, Trp phosphorescence lifetimes are mainly quenched by out-of-plane vibrations of the indole ring (*15*, *16*), resulting in shorter phosphorescence lifetimes for Trp residues in more flexible environments (*17*−*19*). Trp phosphorescence thus provides a local probe for changes in conformational fluctuations due to changes in local flexibility or protein unfolding.

† This work was supported by ARO Grant DAAH04-95-1-0613 (F.H.A.) and by National Institute of Aging Grant AG09761 (J.A.S.).

* Corresponding author: phone 626-395-4162; fax 626-568-8743; e-mail frances@cheme.caltech.edu.

‡ Division of Chemistry & Chemical Engineering, California Institute of Technology.

§ Institute of Gerontology, University of Michigan.

|| Present address: Maxygen, Inc., 515 Galveston Dr., Redwood City, CA 94063.

[1] Abbreviations: DSC, differential scanning calorimetry; DTNB, 5,5′-dithiobis(2-nitrobenzoic acid); MEM, maximum entropy method; *p*NB E, *p*-nitrobenzyl esterase; *p*NPA, *p*-nitrophenyl acetate; CAPS, 3-(cyclohexylamino)-1-propanesulfonic acid; PIPES, piperazine-*N*,*N*′-bis(2-ethanesulfonic acid); TAPS, *N*-tris(hydroxymethyl)methyl-3-aminopropanesulfonic acid.

10.1021/bi992473s CCC: $19.00
Published on Web 03/30/2000

MATERIALS AND METHODS

Directed Evolution. Random mutagenesis, recombination by DNA shuffling, library construction, and thermostability screening assays were performed as described (*11*).

Enzyme Activity. Enzyme activity assays on *p*-nitrophenyl acetate (*p*NPA) in 100 mM PIPES, pH 7.0, were performed using purified, filtered enzyme as described (*20*).

Thermostability. Melting temperatures (T_m) in 100 mM PIPES, pH 7.0, were determined from the peak of the first endotherm in the differential scanning calorimetry (DSC) traces, as described (*11*).

Room-Temperature Phosphorescence. Protein concentrations were calculated using extinction coefficients at 280 nm (ϵ_{280}) calculated according to the method of Pace and coworkers (*21*). For wild-type *p*NB E and variants from generations 4 through 8, $\epsilon_{280} = 78\,965\ M^{-1}\ cm^{-1}$; for generations 1 through 3, $\epsilon_{280} = 77\,475\ M^{-1}\ cm^{-1}$. Protein concentrations of 100−400 nM were used in 100 mM PIPES, pH 7.0, 100 mM TAPS, pH 8.5, 100 mM TAPS, pH 9.0, or 100 mM CAPS, pH 10.0. Phosphorescence decays of deoxygenated samples were collected, and lifetimes were determined as described (*19*). Protein solutions were deoxygenated for 40 min using an automated system that alternates 1 s of ultrapure argon (20 psi) with 0.1 s of vacuum. Samples were equilibrated at the desired temperature and excited by a 10 ns 280 nm pulse generated by frequency-doubling the 560 nm output of a Continuum (Santa Clara, CA) dye laser containing rhodamine 6G. The dye laser was pumped by a frequency-doubled Continuum Surelite Nd:YAG laser. The emission was selected using a 450 nm interference filter and collected by a photomultiplier tube operating in the photon counting mode. The maximum entropy method (MEM) as implemented by software from Photon Technology International (Monmouth Junction, NJ) was used to analyze the phosphorescence decays.

MEM analysis generates phosphorescence lifetime distributions by maximizing the entropy, *S*, where

$$S = -\sum_{i=1}^{N} a_i \log\left\{\frac{a_i}{\sum_{i=1}^{N} a_i}\right\} \quad (1)$$

and a_i is the amplitude of the *i*th lifetime. The magnitude of the amplitude is a measure of the intensity of each lifetime's contribution to the total phosphorescence signal. Multiple peaks in the distribution indicate the presence of multiple-emitting Trp residues. Broad peaks may arise from a distribution of conformational states and/or from multiple Trp residues with similar lifetimes. All of the *p*NB E phosphorescence lifetime distributions contain contributions from lifetimes of 1 ms or less. These signals arise from fluorescence, extremely short-lived phosphorescence, and cuvette luminescence. Since contributions from fluorescence and phosphorescence cannot be distinguished, these extremely short-lived signals were not analyzed further. Exponential fits to the Arrhenius plots were performed using Kaleidagraph (Synergy Software, Reading, PA).

Exposure of Cysteine Residues. The 412 nm absorbance of 5,5′-dithiobis(2-nitrobenzoic acid) (DTNB) was used to monitor the exposure of cysteine residues due to protein unfolding. The change in absorbance of solutions containing 40 μM DTNB and 1−2 μM protein in 100 mM TAPS, pH 8.5, was measured for 1 h at 40 °C. The results from control experiments performed by incubating DTNB in 100 mM TAPS, pH 8.5 at 40 °C, were subtracted from the protein results. The amount of reacted DTNB was calculated using $\epsilon_{412} = 25\,000\ M^{-1}\ cm^{-1}$.

RESULTS

Stability of Evolved pNB Esterases. PCR-based random mutagenesis of sixth-generation thermostable *p*NB esterase variant 6sF9 (*11*) yielded a seventh-generation library, which was expressed in *E. coli* and screened for thermostability. The eighth-generation library was generated by recombining the three most thermostable seventh-generation variants using DNA shuffling. Subsequent DNA sequencing, however, revealed two of the recombined variants to be 6sF9. Only one, 7G5, contained new thermostabilizing mutations. The best mutant from the eighth-generation library, 8G8, has 13 amino acid substitutions relative to wild-type *p*NB E and 4 substitutions with regard to 6sF9. Two mutations, Thr 73 Lys and Thr 459 Ser, originated in 7G5. The other two, Ala 56 Val and Ala 400 Thr, were random mutations that arose during DNA shuffling. Of the 13 mutations, 10, including Thr 73 Lys, have been identified as thermostabilizing by site-directed mutagenesis experiments (*11*) and/or comparisons of the X-ray crystal structures of wild-type and 8G8 *p*NB E (*14*). While Ala 56 Val and/or Ala 400 Thr must be stabilizing in 8G8, they fail to stabilize wild-type *p*NB E when introduced as a double mutation. Structural comparisons of wild type and 8G8 also fail to reveal stabilizing mechanisms for Ala 56 Val, Ala 400 Thr, and Thr 459 Ser (*14*). Since Ala 56 Val and Ala 400 Thr occur in the same generation, and Thr 459 Ser appears with Thr 73 Lys, one or more of these mutations may be neutral.

DSC of *p*NB E wild type and mutants revealed two endotherms (Figure 1A). For all *p*NB E variants, the peaks of the two endotherms are separated by 6−10 °C, and the first endotherm has at least 3 times the amplitude of the second. The peak of the first endotherm (T_m) increases from 52.5 to 69.5 °C over the eight generations, while the peak of the second endotherm increases from 63.5 to 79.0 °C. No endotherm is observed upon repeat scanning of the samples, indicating that *p*NB E does not refold under these conditions. The locations of both peaks depend on the scan rate (data not shown), due to the irreversibility of thermal denaturation.

*p*NB esterases 1A5D1, 2A12, 3H5, 4G4, 5H3, 6sF9, 7G5, and 8G8 are the most fit mutants from generations 1 through 8, respectively. The first number in each designation indicates the generation of origin. With each generation, new amino acid mutations are added (one mutation is lost from 5H3 to 6sF9 due to recombination) and thermostability increases.

Activities of Evolved pNB Esterases. While the natural substrate of *p*NB E is unknown, the wild-type enzyme has measurable activity on several laboratory substrates, including *p*NPA (*20, 22*). 8G8 has the highest activity toward *p*NPA of all the purified *p*NB E variants (Figure 1B). At 30 °C, its activity is 3 times that of wild type, 15 times that of the best first generation mutant, 1A5D1, and 2 times that of

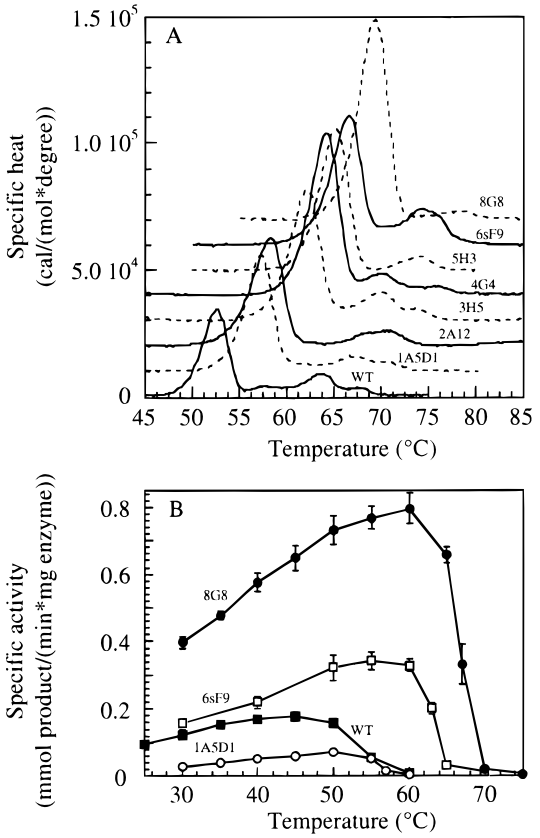

FIGURE 1: (A) DSC of wild-type (WT) and the most thermostable *p*NB E variants from generations 1 (1A5D1), 2 (2A12), 3 (3H5), 4 (4G4), 5 (5H3), 6 (6sF9), and 8 (8G8). As the thermostability of the variants increases, the endotherms move to higher temperatures. All data were collected at a scan rate of 1 °C/min using 14.5−15.5 μM *p*NB E in 100 mM PIPES, pH 7.0. The curves are offset for clarity. (B) Specific activities of WT (■) and evolved esterases 1A5D1 (○), 6sF9 (□), and 8G8 (●) toward *p*NPA in 100 mM PIPES, pH 7.0, as a function of temperature. Measurements are the mean ± standard deviation for at least 3 independent measurements. For temperatures at which the variants were unstable, the activity was measured following a 5 min incubation.

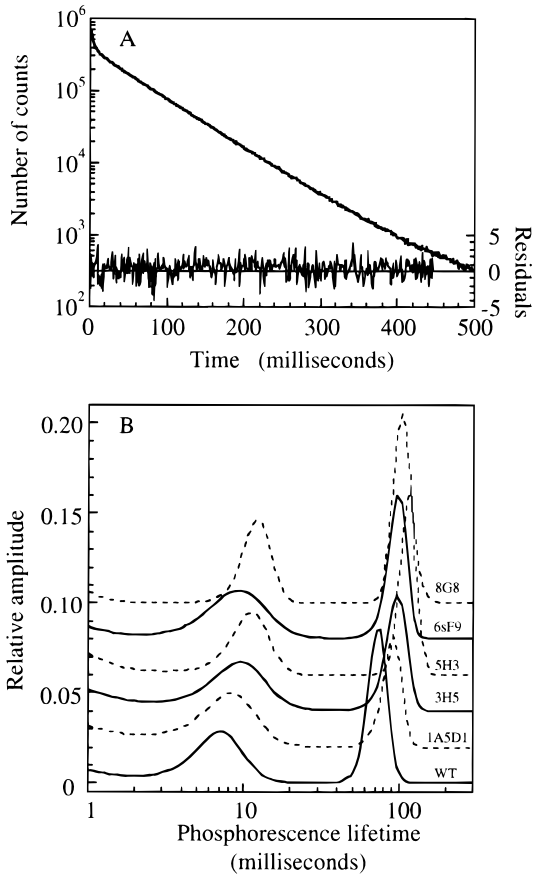

FIGURE 2: (A) Recorded phosphorescence decay of wild-type *p*NB E at 20 °C in 100 mM TAPS, pH 8.5, and the residuals from the fit to the lifetime distribution. (B) Phosphorescence lifetime distributions at 20 °C in 100 mM TAPS, pH 8.5, for wild-type (WT) *p*NB E and the thermostable variants 1A5D1, 3H5, 5H3, 6sF9, and 8G8. The distributions are offset for clarity.

6sF9. The temperature of optimal activity (T_{opt}) of 8G8 is also shifted to higher temperatures: T_{opt} is approximately 60 °C for 8G8 versus 45 °C for wild-type *p*NB E (Figure 1B). This 15 °C increase in T_{opt} follows the increase in T_m, and occurs without changing the general shape of the activity−temperature curve.

Phosphorescence Lifetimes. The time-resolved phosphorescence of wild-type *p*NB E and its thermostable variants was measured at pH values ranging from 7 to 10. With 10 Trp residues, *p*NB E might be expected to display phosphorescence with a multitude of lifetimes. However, the *p*NB E phosphorescence decays have only three major components: an extremely short lifetime (<1 ms) indicative of solvent-exposed Trps and two longer lifetimes (approximately 10 and 100 ms) (Figure 2). The lifetimes of the latter two phosphorescence components increase, as do the enzyme activities, as the pH is raised to 9 (data not shown). At pH 10, the phosphorescence lifetimes decrease, and only the most thermostable mutant 8G8 retains a phosphorescence signal following several hours of incubation (data not shown). The increase in phosphorescence lifetime from pH 7 to 9 is accompanied by a decrease in the width of the long lifetime peak (Figures 2B and 3A). The narrow peaks observed at pH 8.5 and 9 suggest that the long-lived phosphorescence arises from a single Trp residue.

Because out-of-plane vibrations quench Trp phosphorescence, phosphorescing residues must be located in relatively rigid parts of the *p*NB E structure that are sequestered from solvent. The X-ray crystal structures of wild-type, 8G8, and "organophile" 5-6C8 *p*NB E reveal that 2 of the 10 Trp residues (37 and 48) are largely exposed to solvent (*14*) and cannot, therefore, phosphoresce. Trp residues 24, 102, 168, and 364 are the least exposed to solvent in all three structures.

Crystallographic temperature factors can provide a measure of residue flexibility. However, due to crystal heterogeneity and crystal contacts, temperature factors have large associated uncertainties when interpreted in terms of flexibility. While the absolute values of the temperature factors vary between the three *p*NB E structures, they show similar trends. Among the Trp residues in all three structures, Trps 102, 381, and 436 have the lowest temperature factors. Information on residue flexibility can be supplemented by examining the secondary structure. Residues in β sheets are generally more constrained than those in other secondary structures. Trp residues 24, 102, and 381 are located in β strands. Solvent exposure, temperature factors, and location on a β strand point to Trp 102 as the source of the long-lived *p*NB E phosphorescence lifetime.

To further pinpoint the phosphorescing Trp residues, the phosphorescence of the sixth-generation 6sF9 variant was

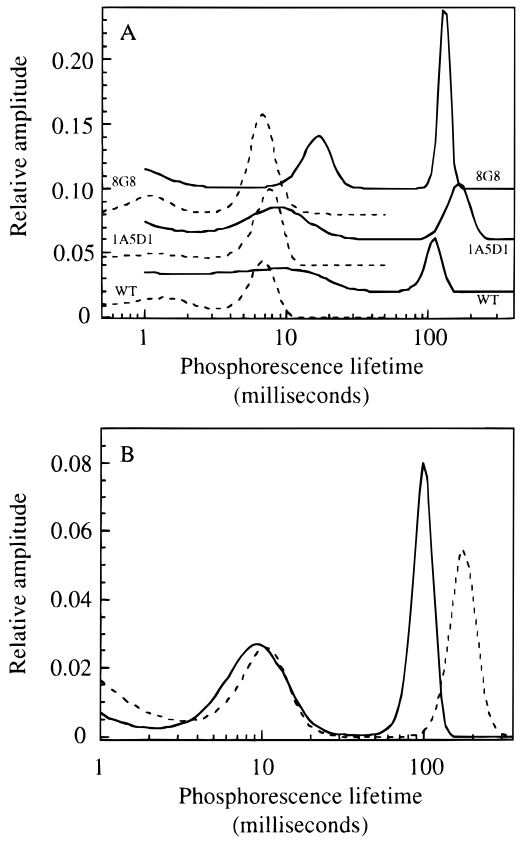

FIGURE 3: (A) Lengthening of phosphorescence lifetimes at 20 °C due to increasing pH for *p*NB E wild-type and thermostable variants 1A5D1 and 8G8. Data collected in 100 mM PIPES, pH 7.0 (- - -), and in 100 mM TAPS, pH 9.0 (—). (B) Phosphorescence lifetimes of thermostable variant 6sF9 in deuterated (- - -) and nondeuterated (—) buffers.

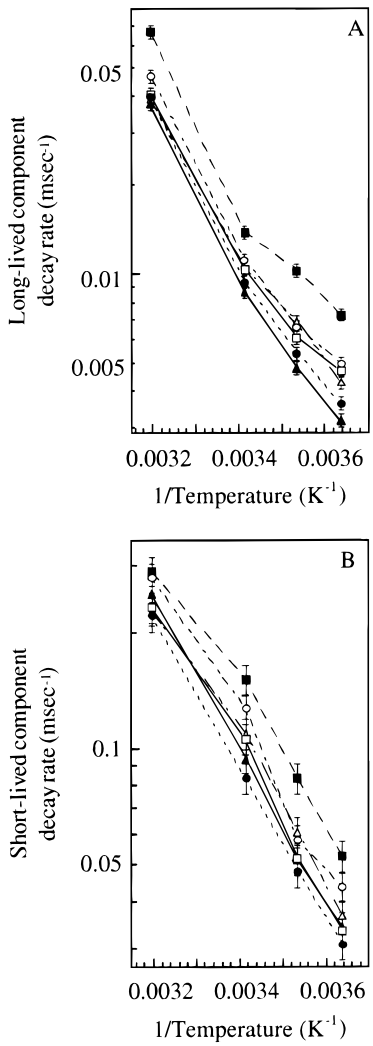

FIGURE 4: Temperature dependence of the phosphorescence decay rates (1/lifetime) for the (A) long-lived and (B) short-lived components at pH 8.5. Displayed are wild-type *p*NB E (■) and the most thermostable esterases from generations 1 (○), 3 (△), 5(▲), 6 (□), and 8 (●).

measured in both deuterated and nondeuterated solvent at pH 8.5 and 20 °C. Room-temperature phosphorescence studies of wild-type and mutant alkaline phosphatase (AP) indicate that deuteration of the tryptophan enamine increases the phosphorescence lifetime (*23*). Further studies of site-directed mutants of AP suggest that the increase in phosphorescence lifetime with deuteration is greater when the indole enamine is not hydrogen-bonded (C. J. Fischer and J. A. Schauerte, unpublished data). A possible explanation for this pattern is that out-of-plane vibrational modes of hydrogen-bonded Trp residues are already damped, lessening the effect of increasing the mass by deuteration. Deuteration of *p*NB E 6sF9 lengthens the average long phosphorescence lifetime from 88 to 173 ms without significantly affecting the short component (Figure 3). *p*NB E Trp residues 24, 102, 387, and 452 are not hydrogen-bonded. Based on the criteria discussed above and the deuteration data, we conclude that Trp 102 is the source of the long lifetime component of the phosphorescence signal.

The identity of the shorter-lived phosphorescent species is less clear. This peak does not bifurcate or broaden significantly when the pH, temperature, or solvent is changed. It is unlikely that multiple Trp residues in disparate parts of the enzyme would react identically to these environmental changes. Based on its insensitivity to environmental parameters and relatively narrow width, we conclude that this phosphorescence signal arises from a single Trp residue or from neighboring Trp residues which experience the same environment. In both deuterated and nondeuterated solvent, the 6sF9 short phosphorescence lifetime averages 9.9 ms (Figure 3), suggesting that the indole enamine participates in a hydrogen bond. Trp residues 168, 364, 381, and 436 are solvent-sequestered and hydrogen-bonded. The low temperature factors of Trps 381 and 436 suggest that the short-lived phosphorescence component arises from one of these two Trp residues, although Trps 168 and 364 cannot be entirely ruled out.

The phosphorescence decays were determined as a function of temperature at pH 7 and pH 8.5 (Figure 4). The amplitudes of the Arrhenius plots at pH 8.5 vary for wild-type and thermostable *p*NB E, but the activation energies are similar. As has been seen for other proteins (*24*, *25*), the long lifetime Arrhenius plots (Figure 4A) fit to two exponentials with activation energies of 2700 (±400) cm^{-1} and 4600 (±300) cm^{-1}. For shorter phosphorescence lifetimes, this second component is difficult to resolve, and the Arrhenius plots (Figure 4B) can be fit with a single activation energy of 3000 (±200) cm^{-1}, which is consistent with the lower activation energy of the long lifetime component.

At pH 7, where the proximity of the two phosphorescence lifetime peaks increases the uncertainty of the measurement, there are no significant differences in phosphorescence lifetimes across the *p*NB esterase lineage (Figure 3). At pH 8.5, however, the peaks are well-resolved, and wild-type *p*NB E consistently has the shortest lifetimes and the most flexible phosphorescent Trp residues (Figures 2 and 4). The difference between wild-type and the thermostable variants is most pronounced for the long-lived component. At all temperatures, the wild-type long lifetime is at least 20% shorter than that of 1A5D1.

While there is a tendency for the more thermostable variants to have longer lifetimes, this correspondence is not perfect. For the short phosphorescence component, 1A5D1 and the third-generation variant 3H5 have the shortest lifetimes, the fifth- and sixth-generation variants 5H3 and 6sF9 have similar, longer lifetimes, and 8G8 has the longest. However, for the long phosphorescence component, the 6sF9 lifetimes are comparable to those of 1A5D1 and 3H5, while both 5H3 and 8G8 have longer lifetimes. At low temperatures, the long lifetime of 5H3 is greater than that of 8G8.

The sum of the amplitudes in a phosphorescence lifetime peak is proportional to the population of chromophores emitting with the same or similar phosphorescence lifetimes. The size of this population is sensitive to events occurring in the singlet state, including nonradiative decay (internal conversion), fluorescence, energy transfer between tryptophans in the singlet state, and the intersystem crossing efficiency into the triplet state. A precise estimate of the phosphorescence quantum yield would require knowledge of the fluorescence lifetimes. All 10 *p*NB E Trp residues are likely to fluoresce, making it extremely difficult to identify signals from individual Trp residues. However, the ratio of quantum efficiencies of distinct lifetime components, as reflected by the ratio of the summed amplitudes, provides information regarding processes that differ between phosphorescent Trp residues. Environmental changes which affect only one of the phosphorescing Trp residues, through changes in the triplet or singlet states or the intersystem crossing rate, will alter the relative quantum yield.

The relative quantum yield, the ratio of the summed long lifetime amplitudes to the summed short lifetime amplitudes, tends to increase with thermostability (Figure 5A). However, in contrast to the phosphorescence lifetimes, wild type is not easily distinguishable from thermostable variants 1A5D1 and 3H5. At 40 °C and pH 8.5, both wild-type *p*NB E and 1A5D1 show large drops in the relative quantum yield, decreases in the long lifetime amplitudes, and the appearance of a new, very short lifetime component (Figure 5B). The lifetime of the original short lifetime component decreases as expected when the temperature is raised. No significant loss in amplitude is observed, indicating that the local environment of the short-lived Trp residue remains undisturbed. At 48 °C, sixth-generation variant 6sF9 also experiences the loss of the long lifetime amplitude. But no detectable changes are seen in the 8G8 phosphorescence lifetime distribution, even up to 55 °C (data not shown). The extremely short component disappears and the long lifetime amplitude is restored when the protein solution is cooled to room temperature; however, prolonged exposure to high temperatures at higher pHs is associated with irreversible loss of the long lifetime peak and of enzymatic activity as well as the retention of the extremely short component. The changes in the phosphorescence lifetime distribution and the loss of enzymatic activity at elevated temperatures are due to partial unfolding of *p*NB E.

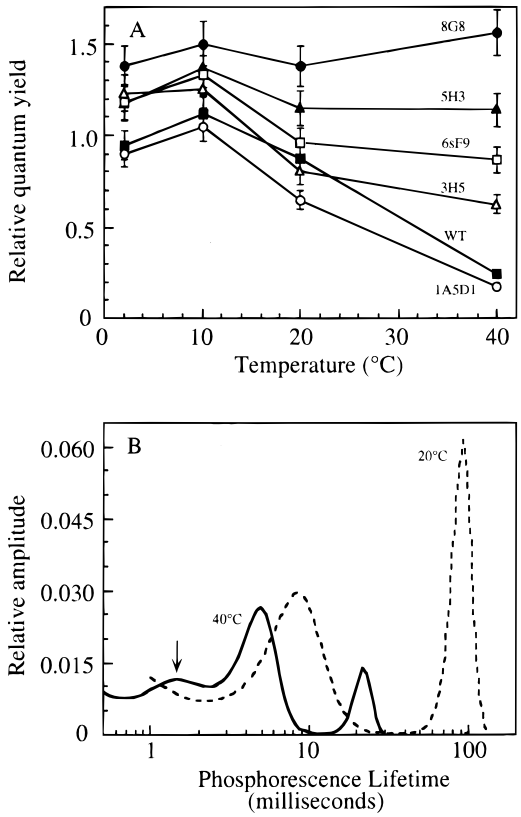

FIGURE 5: (A) Temperature dependence of the relative quantum yield at pH 8.5 for wild-type *p*NB E (■) and the most thermostable esterases from generations 1 (○), 3 (△), 5(▲), 6 (□), and 8 (●). (B) Phosphorescence lifetime distribution of the most thermostable first generation *p*NB E mutant, 1A5D1, at 20 °C (- - -) and 40 °C (—) at pH 8.5. The emergence of a new, extremely short lifetime due to *p*NB E unfolding is indicated by the arrow.

DTNB Reactivity. *p*NB E contains two buried cysteine residues, 61 and 82, in the N-terminal region. Despite their proximity in the three-dimensional structure, they do not form a disulfide bond (*14*). Under denaturing conditions, 4 M guanidine hydrochloride and pH 8.5, the Cys residues are exposed and react with DTNB. DTNB reactivity was monitored at pH 8.5 and 40 °C, where the relative quantum yields of both wild-type and 1A5D1 *p*NB E decrease. Following 1 h of incubation, wild type and 1A5D1 have reactivities toward DTNB of 0.43 and 0.58, respectively, relative to the denatured control. Thermostable variants 6sF9 and 8G8 have relative reactivities of only 0.11 and 0.04, respectively. The relative reactivity of 8G8 is within the experimental uncertainty of the DTNB measurement.

DISCUSSION

Thermostabilities and Activities of Evolved pNB Esterases. Laboratory evolution of *p*NB E required stability at high temperature—70 °C for the eighth generation—simultaneous with high activity at room temperature (*11*). Naturally occurring thermophilic and mesophilic enzymes, in contrast, are not exposed to such wide temperature ranges. Thus, there is no evolutionary pressure for mesophilic enzymes to be stable at high temperature or thermophilic enzymes to be

active at low temperature. In fact, excess stability could interfere with the cell's ability to regulate enzyme levels. Significant low-temperature activity would lead to extremely high activity at elevated temperature (see, for example, ref *26*) which could be detrimental to a thermophilic organism. Thus, for many naturally occurring enzymes, there is an apparent tradeoff between thermal stability and low-temperature activity.

However, these properties can be combined in laboratory-evolved enzymes. The best eighth-generation *p*NB E 8G8 has a T_m 17 °C higher than the wild type. This increase in thermostability is equivalent to the difference in stability between some thermophilic and mesophilic enzymes (*6*, *7*). At the same time, there is a gain rather than loss of low-temperature activity relative to its mesophilic progenitor. At 30 °C, 8G8's catalytic efficiency is 3.5 times that of wild type, and its optimal activity is 4.5 times higher. Evolution in the laboratory has resulted in similar thermostability and activity increases for mesophilic subtilisin E (*13*) and psychrophilic subtilisin S41 (K. Miyazaki, personal communication). The tradeoffs often observed in natural enzymes clearly do not reflect physicochemical limitations.

Enzyme Flexibility, Activity, and Stability. Changes in Trp phosphorescence reflect changes in the local environment of solvent-sequestered Trp residues. Trp phosphorescence is primarily quenched by vibrational coupling between the Trp triplet and ground states due to out-of-plane distortions of the aromatic ring (*15*, *16*). These out-of-plane distortions, which occur on the picosecond time scale (*27*), are influenced by the local environment, so that Trp residues in more densely packed regions and in β sheets have smaller amplitude vibrations and longer lifetimes. In addition, larger-scale motions such as breathing motions or local unfolding that occur during the phosphorescence lifetimes (which range from milliseconds to hundreds of milliseconds for *p*NB E) can quench the phosphorescence. Variants with higher rates of transient unfolding will have shorter phosphorescence lifetimes.

The activation energies derived from the Arrhenius plots demonstrate that the triplet state decay processes are similar for wild-type and variant *p*NB Es. Indeed, the *p*NB E phosphorescence lifetime Arrhenius plots resemble those observed for other proteins (*24*, *25*), indicating a common deactivation mechanism. The nonlinearity of the Arrhenius plot, particularly evident for the long phosphorescence lifetime (Figure 4A), has also been observed with other proteins (*24*, *25*) and has been attributed to activation of large-scale motions at higher temperatures (*25*). An alternate explanation, consistent with the behavior of other aromatic molecules (*28*, *29*), is the activation at higher temperatures of multiple vibrational modes capable of nonradiative deactivation.

The wild-type and two mutant crystal structures (*14*) show no evidence for significant changes in distances or orientations between the phosphorescing Trp residues and other amino acids that may quench Trp phosphorescence. Nor are the two mutations, His 322 Tyr and Tyr 370 Phe, which could result in differences in quenching close to any of the phosphorescing Trp residues. Thus, this system should be appropriate for investigating relationships between flexibility, thermostability, and catalytic activity.

The thermostable variants have catalytic efficiencies toward *p*NPA which, at 30 °C, are 4.0−3.5 times less than

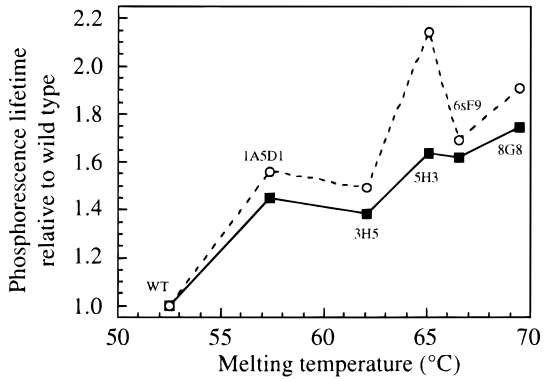

FIGURE 6: Relationships between phosphorescence lifetimes and thermostability for wild-type *p*NB E and the most thermostable variants from generations 1, 3, 5, 6, and 8 at pH 8.5 and 20 °C. All variants are normalized to the wild-type values. The short (■) and long (○) lifetimes are displayed.

wild type for 1A5D1 and 3H5 and 1.5−3.5 times greater than wild type for 5H3, 6sF9, and 8G8. Comparisons between thermophilic and mesophilic homologues of 3-phosphoglycerate kinase (*6*) and 3-isopropylmalate dehydrogenase (*7*) suggest that decreased activity is correlated with decreased flexibility. If this were true for the *p*NB E lineage, then 1A5D1 and 3H5 would have the longest phosphorescence lifetimes, 8G8 would have the shortest lifetimes, and the wild type, 5H3, and 6sF9 lifetimes would fall somewhere in between. In fact, at pH 8.5, where the separation between the short and long lifetimes is better resolved than at pH 7.0, wild-type *p*NB E has shorter phosphorescence lifetimes than any of the thermostable mutants at all temperatures, and 8G8 has some of the longest lifetimes. We therefore conclude that changes in enzyme flexibility in the vicinity of the phosphorescing Trp residues do not influence catalytic activity.

Although phosphorescence lifetimes do not correlate with enzyme activities, we do observe an association with stability (Figures 4 and 6). Wild type consistently has the shortest lifetimes (most flexibility). The variants from the early generations also tend to have shorter lifetimes than their more thermostable descendants. This association is not perfect: the lifetime of the long-lived phosphorescence component for variant 5H3 is greater than for 6sF9 and 8G8. The long 5H3 lifetime as well as the sometimes anomalous behavior of 6sF9 suggests that at least some changes in flexibility are neutral with respect to thermostability.

The significant increase in the phosphorescence lifetimes between wild-type *p*NB E and 1A5D1 may be associated with the 5 °C increase in T_m in this variant. Despite the increasing phosphorescence lifetimes from wild-type *p*NB E to 1A5D1, the relative quantum yields are quite similar, particularly at low temperature. The relative quantum yield is a measure of the difference in local environment between the phosphorescing Trp residues. The agreement between the wild-type and 1A5D1 relative quantum yields, despite differences in lifetimes, suggests that mutations in 1A5D1 have similar effects on both of the phosphorescing Trp residues. The *p*NB E crystal structures suggest a source for this simultaneous decrease in flexibility. Two protein segments, consisting of residues 64−71 and 413−417, have no electron density in the wild-type crystal structure. These loops are stabilized in the structures of 8G8 and the "organophile"

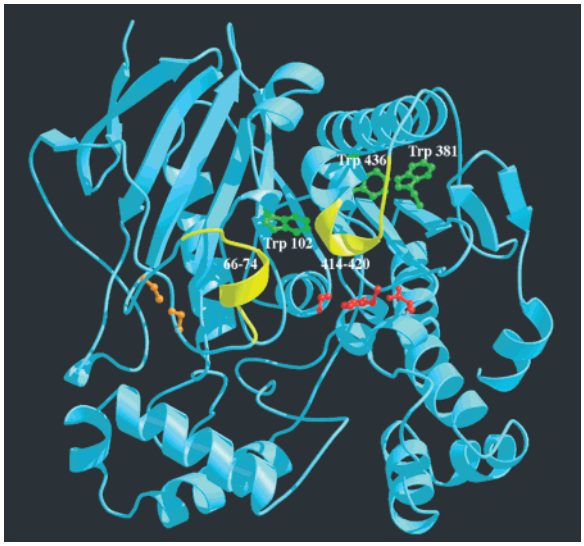

FIGURE 7: Ribbon diagram of the *p*NB E 8G8 X-ray crystal structure (*14*). The flexible loops that become constrained in variant 1A5D1 are shown in yellow. The catalytic triad is in red, the phosphorescing Trp residues are in green, and the Cys residues, which can react with DTNB when exposed to solvent, are shown in orange. Generated with Molscript (*40*) and Raster3D (*41*).

5-6C8 that was evolved for activity in dimethylformamide (*14*). All five mutations in 1A5D1 are found in 5-6C8 (*11*, *30*), and neither of the two mutations unique to 5-6C8 is directly associated with stabilizing the unstructured regions (*14*). Thus, we conclude that these loops are already fixed in 1A5D1. This fixation affects the phosphorescence of distant Trp residues (Figure 7).

Mutational studies suggest that long-range interactions are involved in the *p*NB E loop stabilization. The Ile 60 Val substitution, which stabilizes unstructured residues by allowing the loop from 66 to 74 to pack against residues 60−63 (*14*), was discovered in a mutant library generated during evolution of the organophile 5-6C8 and later screened for thermostability (*11*). The parent of this library contained three substitutions: His 322 Arg, Met 358 Val, and Tyr 370 Phe. In this background, the two new mutations in 1A5D1, Ile 60 Val and Leu 144 Met, are stabilizing as either single or double mutations. However, both fail to stabilize wild-type *p*NB E when introduced as single mutations (*11*). His 322 Arg, Met 358 Val, and Tyr 370 Phe are all located at least 20 Å from Ile 60 Val and Leu 144 Met, demonstrating that cooperative interactions between distant parts of the protein help to stabilize the formerly unstructured loops. With the exception of Trp 364, all of the Trp residues are also located far from the mutations; therefore, differences in phosphorescence lifetimes between the wild type and thermostable mutants could arise from these same long-range, cooperative interactions. The ability of long-range interactions to stabilize loops was also demonstrated for dihydrofolate reductase, where two loop-associated mutations were destabilizing individually but stabilizing as a double mutation, despite a separation of 28 Å (*31*).

From the phosphorescence and X-ray structural data, we see that the cooperative interactions which stabilize the loop conformations are associated with a decrease in flexibility in the loop regions as well as in the distant parts of the enzyme where the Trp residues are located. While reducing mobility has an entropic cost that can decrease stability (*2*), the burial of hydrophobic residues, introduction of new hydrogen bonds, and restriction of solvent accessibility to the protein core due to the structuring of the loop regions apparently counteract this cost and stabilize *p*NB E. Similar results were seen for *Bacillus polymyxa* β-glucosidase A, where a single, thermostabilizing mutation restricted the mobility of approximately 100 amino acid residues around the mutation (*32*). Restriction of loop motion has also been associated with the thermostabilization of *Bacillus subtilis* subtilisin E (*4*).

Decreased flexibility, however, can also be accompanied by decreased stability. All of the *p*NB esterases display decreases in thermostability from pH 7 to 9 while the phosphorescence lifetimes increase. While decreases in thermostability with increasing pH may arise primarily from changes in electrostatic interactions, the entropic cost of reduced flexibility (*2*) may also play a role.

pNB E Unfolding. At pH 8.5 and 40 °C, wild-type *p*NB E and 1A5D1 both show a drop in the relative quantum yield, and an extremely short lifetime component appears. The original short lifetime component does not change significantly. Thermostable variant 6sF9 shows similar behavior at 48 °C. The loss of the long lifetime amplitude and the appearance of the new component occur not through a gradual shortening of the long lifetime but as a two-state transition from a long phosphorescence lifetime to an extremely short lifetime. Similar reductions in phosphorescence lifetimes seen in the unfolding of *E. coli* alkaline phosphatase have been attributed to folding intermediates (*33*). The most likely source of this transition in *p*NB E is the preferential unfolding of the region surrounding the long-lived Trp, which occurs at relatively low temperatures for wild type and its least thermostable variants.

The multiple endotherms in the DSC traces also indicate the presence of unfolding intermediates in *p*NB E. Multiple endotherms were observed during the thermal unfolding of equine lysozyme and staphylococcal nuclease, enzymes in which different regions unfold independently (*34*). In equine lysozyme, the independent folding domains are separated by the active site cleft (*35*). Similar thermal denaturation behavior was seen in papain (*36*), although the difference in melting temperatures of the papain domains is not large enough to lead to separate DSC peaks (*37*). Although *p*NB E is a single-domain protein, it does have a prominent active site cleft similar to the active site "gorge" in the homologous enzyme acetylcholinesterase (*14*, *38*). This cleft divides the protein into a larger N-terminal region and a smaller C-terminal region that could unfold independently.

Trp 102, the proposed source of the long-lived phosphorescence lifetime, is located in the N-terminal region (Figure 7). Thus, the loss of the long-lived phosphorescence component indicates that the N-terminal region unfolds first upon thermal denaturation. Thermolability of the N-terminal region is supported by the results of the DTNB experiments. Both of the cysteine residues in *p*NB E are located in the N-terminal region, and increased accessibility of these residues and loss of the long-lived phosphorescence occur under the same conditions.

Surprisingly, only 3 of the 10 identified thermostabilizing amino acid substitutions occur in the apparently more thermolabile N-terminal region (Ile 60 Val, Thr 73 Lys, and Leu 144 Met). All of these fail to stabilize wild-type *p*NB E

when introduced singly, although they are stabilizing when C-terminal mutations are present. Thus, while the observable structural changes due to the seven thermostabilizing C-terminal mutations are localized (*14*), their effects may well propagate across the active site cleft. This propagation may occur through dynamic rather than static changes in *p*NB E.

The ability of amino acid mutations to affect distant parts of a protein has also been observed during the *in vitro* evolution of enzyme activity. Laboratory evolution of *p*NB E (*20, 30*) and aspartate aminotransferase (*39*) resulted in mutants with substantially increased activities toward unnatural substrates. All of the mutations occurred far, often more than 20 Å, from the active site. Enzymes are complex molecules in which cooperative interactions lead to the propagation of mutational effects over large distances. This behavior makes it difficult to predict the effects of mutations, a complication that is circumvented by using evolutionary approaches to protein engineering.

ACKNOWLEDGMENT

We thank Dr. Patrick L. Wintrode for helpful discussions and comments. We also thank Dr. Kentaro Miyazki and Christopher J. Fischer for access to data prior to publication.

REFERENCES

1. Wrba, A., Schweiger, A., Schultes, V., Jaenicke, R., and Závodszky, P. (1990) *Biochemistry 29*, 7584−7592.
2. Lazaridis, T., Lee, I., and Karplus, M. (1997) *Protein Sci. 6*, 2589−2605.
3. Lumry, R., and Rajender, S. (1970) *Biopolymers*, 1125−1227.
4. Colombo, G., and Merz, K. M. (1999) *J. Am. Chem. Soc. 121*, 6895−6903.
5. Jaenicke, R., and Závodszky, P. (1990) *FEBS Lett. 268*, 344−349.
6. Varley, P. G., and Pain, R. H. (1991) *J. Mol. Biol. 220*, 531−538.
7. Závodszky, P., Kardos, J., Svingor, A., and Petsko, G. A. (1998) *Proc. Natl. Acad. Sci. U.S.A. 95*, 7406−7411.
8. Kohen, A., Cannio, R., Bartolucci, S., and Klinman, J. P. (1999) *Nature 399*, 496−499.
9. Akanuma, S., Yamagishi, A., Tanaka, N., and Oshima, T. (1998) *Protein Sci. 7*, 698−705.
10. Akanuma, S., Yamagishi, A., Tanaka, N., and Oshima, T. (1999) *Eur. J. Biochem. 260*, 499−504.
11. Giver, L., Gershenson, A., Freskgard, P. O., and Arnold, F. H. (1998) *Proc. Natl. Acad. Sci. U.S.A. 95*, 12809−12813.
12. Rellos, P., Pinheiro, L., and Scopes, R. K. (1998) *Protein Expression Purif. 12*, 61−66.
13. Zhao, H. M., and Arnold, F. H. (1999) *Protein Eng. 12*, 47−53.
14. Spiller, B., Gershenson, A., Arnold, F. H., and Stevens, R. C. (1999) *Proc. Nat. Acad. Sci. U.S.A. 96*, 12305−12310.
15. Lower, S. K., and El-Sayed, M. A. (1966) *Chem. Rev. 66*, 199−241.
16. McGlynn, S. P., Azumi, T., and Kinosita, M. (1969) *Molecular Spectroscopy of the Triplet State*, Prentice-Hall, Englewood Cliffs, NJ.
17. Papp, S., and Vanderkooi, J. M. (1989) *Photochem. Photobiol. 49*, 775−784.
18. Strambini, G. B., and Gonnelli, M. (1985) *Chem. Phys. Lett. 115*, 196−200.
19. Schauerte, J. A., Steel, D. G., and Gafni, A. (1997) *Methods Enzymol. 278*, 49−71.
20. Moore, J. C., and Arnold, F. H. (1996) *Nat. Biotechnol. 14*, 458−467.
21. Pace, C. N., Vajdos, F., Fee, L., Grimsley, G., and Gray, T. (1995) *Protein Sci. 4*, 2411−2423.
22. Chen, Y. R., Usui, S., Queener, S. W., and Yu, C. A. (1995) *J. Ind. Microbiol. 15*, 10−18.
23. Fischer, C. J., Schauerte, J. A., Wisser, K. C., Gafni, A., and Steel, D. G. (2000) *Biochemistry 39*, 1455−1461.
24. Vanderkooi, J. M., Owen, C. S., and Wright, W. W. (1992) *Proc. SPIE−Int. Soc. Opt. Eng. 1640*, 473−477.
25. Tölgyesi, F., Ullrich, B., and Fidy, J. (1999) *Biochim. Biophys. Acta 1435*, 1−6.
26. Merz, A., Knochel, T., Jansonius, J. N., and Kirschner, K. (1999) *J. Mol. Biol. 288*, 753−763.
27. Brooks, C. L., Karplus, M., and Pettitt, B. M. (1988) *Proteins: A theoretical perspective on dynamics, structure, and thermodynamics*, John Wiley & Sons, New York.
28. Kono, H., Lin, S. H., and Schlag, E. W. (1988) *Chem. Phys. Lett. 145*, 280−285.
29. Sobolewski, A. L., Lim, E. C., and Siebrand, W. (1991) *Int. J. Quantum Chem. 39*, 309−324.
30. Moore, J. C., Jin, H. M., Kuchner, O., and Arnold, F. H. (1997) *J. Mol. Biol. 272*, 336−347.
31. Ohmae, E., Iriyama, K., Ichihara, S., and Gekko, K. (1998) *J. Biochem. 123*, 33−41.
32. Sanz-Aparicio, J., Hermoso, J., Martinez-Ripoll, M., Gonzalez, B., Lopez-Camacho, C., and Polaina, J. (1998) *Proteins: Struct., Funct., Genet. 33*, 567−576.
33. Mersol, J. V., Steel, D. G., and Gafni, A. (1993) *Biophys. Chem. 48*, 281−291.
34. Privalov, P. L. (1996) *J. Mol. Biol. 258*, 707−725.
35. Griko, Y. V., Freire, E., Privalov, G., Vandael, H., and Privalov, P. L. (1995) *J. Mol. Biol. 252*, 447−459.
36. Hernández-Arana, A., and Soriano-Garcia, M. (1988) *Biochim. Biophys. Acta 954*, 170−175.
37. Tiktopulo, E. L., and Privalov, P. L. (1978) *FEBS Lett. 91*, 57−58.
38. Sussman, J. L., Harel, M., Frolow, F., Oefner, C., Goldman, A., Toker, L., and Silman, I. (1991) *Science 253*, 872−879.
39. Oue, S., Okamoto, A., Yano, T., and Kagamiyama, H. (1999) *J. Biol. Chem. 274*, 2344−2349.
40. Kraulis, P. J. (1991) *J. Appl. Crystallogr. 24*, 946−950.
41. Merritt, E. A., and Murphy, M. E. P. (1994) *Acta Crystallogr. D 50*, 869−873.

BI992473S